Multivalley dark solitons in multicomponent Bose-Einstein condensates with repulsive interactions

Yan-Hong Qin,[1,3] Li-Chen Zhao,[1,2,3,*] Zeng-Qiang Yang,[4] and Liming Ling[5,†]

[1]*School of Physics, Northwest University, Xi'an 710127, China*
[2]*NSFC-SPTP Peng Huanwu Center for Fundamental Theory, Xi'an 710127, China*
[3]*Shaanxi Key Laboratory for Theoretical Physics Frontiers, Xi'an 710127, China*
[4]*Department of Physics, School of Arts and Sciences, Shaanxi University of Science and Technology, Xi'an 710021, China*
[5]*School of Mathematics, South China University of Technology, Guangzhou 510640, China*

(Received 12 February 2021; revised 8 May 2021; accepted 9 June 2021; published 2 July 2021)

We obtain multivalley dark soliton solutions with asymmetric or symmetric profiles in multicomponent repulsive Bose-Einstein condensates by developing the Darboux transformation method. We demonstrate that the width-dependent parameters of solitons significantly affect the velocity ranges and phase jump regions of multivalley dark solitons, in sharp contrast to scalar dark solitons. For double-valley dark solitons, we find that the phase jump is in the range $[0, 2\pi]$, which is quite different from that of the usual single-valley dark soliton. Based on our results, we argue that the phase jump of an n-valley dark soliton could be in the range $[0, n\pi]$, supported by our analysis extending up to five-component condensates. The interaction between a double-valley dark soliton and a single-valley dark soliton is further investigated, and we reveal a striking collision process in which the double-valley dark soliton is transformed into a breather after colliding with the single-valley dark soliton. Our analyses suggest that this breather transition exists widely in the collision processes involving multivalley dark solitons. The possibilities for observing these multivalley dark solitons in related Bose-Einstein condensates experiments are discussed.

DOI: 10.1103/PhysRevE.104.014201

I. INTRODUCTION

Multicomponent Bose-Einstein condensates (BECs) provide a good platform for the investigation of vector solitons both theoretically and experimentally [1–3] due to the abundance of intra- and interatomic interactions. Various vector solitons have been investigated in multicomponent BECs with attractive or repulsive interactions [2–18]. The major theme of research on attractive BECs is bright solitons [2,6,7,9], while studies on dark solitons (i.e., bright-dark solitons) are considerably hampered by their background modulation instability [19]. This characteristic makes it difficult to observe dark solitons experimentally in attractive BECs.

In contrast, many more dark vector solitons have been experimentally observed in multicomponent repulsive BECs, such as dark-dark solitons [4,10,14], dark-bright solitons [5,8,11,13], dark-antidark solitons [12], dark-dark-bright solitons, and dark-bright-bright solitons [15]. Very recently, experimental observations of the collisions of bright-dark-bright solitons were realized in three-component BECs with repulsive interactions [16]. Nevertheless, the dark solitons in the above-mentioned works refer mainly to single-valley dark solitons (SVDSs). Therefore, we aim to look for multivalley dark soliton (MVDS) solutions in repulsive BECs.

In this work, we present the exact MVDS solutions in multicomponent BECs with repulsive interactions by further developing the Darboux transformation (DT) method. The explicit soliton solutions admit an MVDS in one of the components and multihump bright solitons in the other components. In particular, the soliton width-dependent parameters have a considerable impact on both the velocity range and the phase jump of the MVDS. The phase jump of a double-valley (triple-valley) dark soliton can vary in the range of $[0, 2\pi]$ ($[0, 3\pi]$). These characteristics of MVDS are distinct from the well-known scalar dark soliton, for which the width depends on the velocity and the phase jump can be varied in the range $[0, \pi]$[20–22]. Furthermore, we explore the collision dynamics of MVDSs. The interaction between two MVDSs reflects the density profile variations only after a collision. Interestingly, one MVDS can transition to a breather after colliding with an SVDS; this can occur because the mixture of the effective energies of solitons in all components emerges during the collision process. This breather transition occurs extensively in collision processes involving MVDSs. These findings provide an important supplement for recent reports on nondegenerate solitons [23–26]. We expect that more abundant MVDSs could exist in coupled BECs comprising more components and that the phase jump of an n-valley dark soliton could be in the range of $[0, n\pi]$.

The remainder of this paper is organized as follows. In Sec. II, we introduce the theoretical model and present the double-valley dark soliton (DVDS) solutions in three-component repulsive BECs; we further show the density profiles and analyze the phase features of DVDSs. In Sec. III, we investigate the collision dynamics of DVDSs and report the striking state transition dynamics when they collide with SVDSs. In

*zhaolichen3@nwu.edu.cn
†linglm@scut.edu.cn

Sec. IV, we extend our study to four-component repulsive BECs, where triple-valley dark solitons (TVDSs) can be obtained. Finally, the conclusions and discussion are presented in Sec. V.

II. DOUBLE-VALLEY DARK SOLITONS IN THREE-COMPONENT REPULSIVE CONDENSATES

A. Physical model and double-valley dark soliton solutions

Dark solitons usually admit single valley based on the existing methods, such as the inverse scattering method [27,28], DT method [29,30], Hirota's method [31,32], Kadomtsev-Petviashvili reduction method [33,34], and Bäcklund transformation [35]. We note that it is difficult to obtain dark solitons with more than single valley in $N(N \leqslant 2)$-component nonlinear systems. Therefore, we first attempt to find MVDSs in three-component BECs with repulsive interactions, through further developing DT method [24]. At sufficiently low temperatures and in the framework of the mean-field approach, quasi-one-dimensional three-component repulsive BECs (elongated along the x direction) are well described by the three-component Manakov model [16]:

$$iq_{j,t} + \tfrac{1}{2}q_{j,xx} - (|q_1|^2 + |q_2|^2 + |q_3|^2)q_j = 0, \tag{1}$$

where $q_j(x,t)(j = 1, 2, 3)$ represents the mean-field wave functions of three-component repulsive BECs. The details of the deviation of the dimensionless model Eq. (1) from the original mean-field Gross-Pitaevskii equation can refer to the Supplemental Material in Ref. [16]. This model can also be used to describe the evolution of light in defocusing nonlinear optical fibers [20,21]. A recent experiment on bright-dark-bright solitons in repulsive BECs strongly supports the applicability of the above integrable repulsive three-component Manakov model to three-component BECs with repulsive interactions [16]. For their attractive counterpart, single-hump bright soliton solutions [29,31,36,37] and even multihump bright soliton solutions have been obtained in a multicomponent Manakov system by the Hirota method [23,25,26], DT method [24], and other methods [38,39]. Next, we systematically seek the MVDS solutions in the multicomponent repulsive Manakov model.

The DT method is an effective and convenient way to derive localized wave solutions [40–45]. Recently, it was reported that SVDSs can be obtained through the DT method for multicomponent repulsive Manakov systems [44]. In this paper, we further develop the DT method [44] to derive MVDS solutions in combination with the multifold DT for deriving nondegenerate bright solitons [24]. We find that MVDSs can be derived by performing a multifold DT with some special constraint conditions on the eigenfunctions of the Lax pair. For example, one DVDS can be obtained by performing a twofold DT with the spectral parameters written as $\lambda_j = \frac{1}{2}(\xi_j + \frac{1}{\xi_j})$ and adding some special constraint conditions to the eigenfunctions. The complex parameter $\xi_j = -v_1 + iw_j(j = 1, 2)$ is introduced to simplify the soliton solution and facilitate the analysis of physical meaning of each parameter; the real part determines the soliton's velocity, while the imaginary part is called a soliton width-dependent parameter. The detailed derivations of exact DVDS solutions are given in Appendix A. For the DVDS solutions Eq. (A13), one DVDS is admitted in the first component, and one double-hump bright soliton is allowed in the other two components (DBBS). By simplifying Eq. (A13), the exact general soliton solutions can be expressed as follows:

$$q_1 = \frac{N_1}{M_1}e^{-it}, \tag{2a}$$

$$q_2 = -i2w_1\sqrt{1 - v_1^2 - w_1^2}\frac{\alpha_1}{\xi_1}\frac{N_2}{M_1}e^{i\left[v_1 x - \frac{1}{2}(2+v_1^2-w_1^2)t\right]}, \tag{2b}$$

$$q_3 = -i2w_2\sqrt{1 - v_1^2 - w_2^2}\frac{\beta_2}{\xi_2}\frac{N_3}{M_1}e^{i\left[v_1 x - \frac{1}{2}(2+v_1^2-w_2^2)t\right]}, \tag{2c}$$

with

$$\begin{aligned}
N_1 &= \left[\frac{\xi_2^*}{\xi_2}\alpha_1^2 e^{\kappa_1-\kappa_2} + \frac{\xi_1^*}{\xi_1}\beta_2^2 e^{\kappa_2-\kappa_1} + \alpha_1^2\beta_2^2 e^{\kappa_1+\kappa_2}\right] \\
&\quad \times (w_1+w_2)^2 + \frac{\xi_1^*\xi_2^*}{\xi_1\xi_2}(w_1-w_2)^2 e^{-\kappa_1-\kappa_2}, \\
N_2 &= (w_1+w_2)\left[\beta_2^2(w_1+w_2)e^{\kappa_2} + (w_1-w_2)e^{-\kappa_2}\right], \\
N_3 &= (w_1+w_2)\left[\beta_2^2(w_1+w_2)e^{\kappa_1} + (w_2-w_1)e^{-\kappa_1}\right], \\
M_1 &= \left[\alpha_1^2\beta_2^2 e^{\kappa_1+\kappa_2} + \alpha_1^2 e^{\kappa_1-\kappa_2} + \beta_2^2 e^{\kappa_2-\kappa_1}\right](w_1+w_2)^2 \\
&\quad + (w_1-w_2)^2 e^{-\kappa_1-\kappa_2}, \\
\kappa_1 &= w_1(x - v_1 t), \quad \xi_1 = -v_1 + iw_1, \\
\kappa_2 &= w_2(x - v_1 t), \quad \xi_2 = -v_1 + iw_2,
\end{aligned}$$

where α_1, β_2, v_1, w_1, and w_2 are arbitrary real constants. Among them, the parameters w_1 and w_2 are two soliton width-dependent parameters ($w_1 \neq w_2$). The parameter v_1 is moving velocity, which must satisfy the constraint condition $v_1^2 + w_m^2 < 1$, where w_m is the larger of the two width-dependent parameters, meaning that the soliton width-dependent parameters affect the velocity range. In contrast, the width of a scalar dark soliton depends on the velocity, which cannot exceed the speed of sound [3,20–22]. The parameters α_1 and β_2 are two free parameters related to the relative valley values and the center positions of the two valleys. These parameters nontriviall contribute to the soliton profiles.

B. Density profiles of double-valley dark solitons

The solution expressed in Eq. (2) is generally asymmetric but becomes symmetric when the two free parameters satisfy the condition $\alpha_1 = \beta_2 = \sqrt{(w_2 - w_1)/(w_1 + w_2)}$. Examples of asymmetric and symmetric DBBS solutions are shown in Fig. 1 with solid lines and dashed lines, respectively. The plots from left to right correspond to component q_1, component q_2 and component q_3, respectively. For the asymmetric case depicted in Figs. 1(a1)–1(a3), the parameters are $v_1 = 0.1$, $w_1 = 0.2$, $v_3 = 0.3$, $\alpha_1 = 0.5$, and $\beta_2 = 0.2$. We can see that a DVDS emerges in component q_1, manifesting two spatially localized density "dips" on a uniform background. An asymmetric double-hump bright soliton with one node is exhibited in component q_2, and an asymmetric single-hump bright soliton without a node presents in component q_3 [46]; these two bright solitons are quite different from the fundamental dark-bright-bright soliton observed in Refs. [15,16]. As shown in Fig. 1(a1), two valleys of the asymmetric DVDS are not

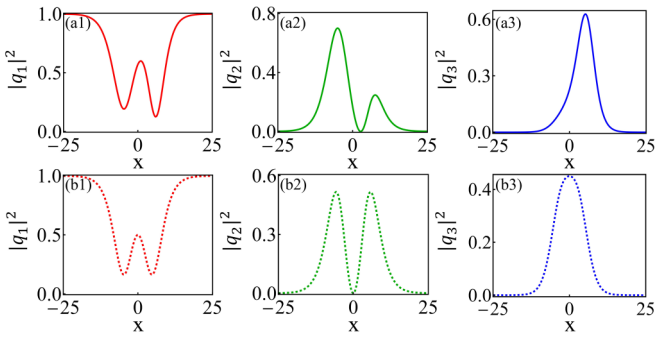

FIG. 1. The density profiles of DVDSs. Panel (a1) shows an asymmetric DVDS in component q_1. Panels (a2, a3) show the density profiles of asymmetric bright solitons in components q_2 and q_3, respectively. Panels (b1–b3) show the corresponding symmetric soliton profiles. The parameters are $\alpha_1 = 0.5$, $\beta_2 = 0.2$ for asymmetric solitons (a1–a3) and $\alpha_1 = \beta_2 = 1/\sqrt{5}$ for symmetric solitons (b1–b3). The other parameters are chosen as $v_1 = 0.1$, $w_1 = 0.2$, and $w_2 = 0.3$.

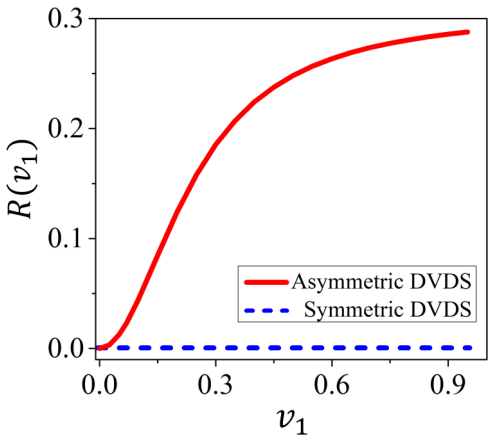

FIG. 2. The asymmetry degree vs moving velocity for DVDSs. The red solid line and blue dashed line correspond to the asymmetric and symmetric DVDSs, respectively. The asymmetry degree increases with increasing moving velocity for asymmetric DVDSs. However, that for symmetric DVDSs remains symmetric with varying velocity. The other parameters are the same as described in the caption of Fig. 1.

equal in either the width or the valley values, in sharp contrast to dark solitons reported in previous studies [2–5,8,10–17,20,21,31–34,44,47]. This characteristic is not observed for the stationary symmetric MVDS solution [48], which was reported to exist in focusing photorefractive media (similar to attractive multicomponent BECs). The bright solitons that present in components q_2 and q_3 are similar to those obtained in a two-component attractive (focusing) system [23–26].

By setting the parameters $\alpha_1 = \beta_2 = \frac{\sqrt{w_2 - w_1}}{\sqrt{w_2 + w_1}}$ and the other parameters the same as in the asymmetric case, the solution Eq. (2) admits symmetric soliton profiles. It has been shown in Figs. 1(b1)–1(b3). These profiles are similar to those reported in previous studies [39,48], but the total density can differ from the "sech-squared" form. Moreover, the DVDS solution is expressed by exponential functions, which is distinctly different from the expressions with associated Legendre polynomials [48]. Moreover, the above DVDS solution is more general than those given in Refs. [39,48] since it admits more free physical parameters. When the width-dependent parameters of soliton w_1 and w_2 are close to each other, both components q_2 and q_3 can show a symmetric (or an asymmetric) double-hump bright soliton. The soliton velocity of the solution in Eq. (2) changes in the range of $[0, \sqrt{1 - w_m^2})$. In particular, the interaction between the solitons can be investigated analytically with further iterations by applying the developing DT method.

Importantly, it must be pointed out that the presence of DVDS makes nondegenerate bright solitons in the other components be different from the ones reported in a attractive (focusing) system [23–26], although they have similar density profiles. For the above nondegenerate solitons Eq. (2), the width-dependent parameters have a dramatic effect on the velocity ranges, and the density profiles of nondegenerate bright solitons depend on the moving velocity. These characters are absent for nondegenerate bright solitons reported before [23–26]. In addition, DVDS-related nondegenerate solitons can also be deduced in attractive system, where the soliton parameters are totally unrestricted. However, the modulation instability of background field of DVDS induce the solitons be unstable and hard to be observed in experiments. On the other hand, the variation of background amplitude of DVDS will cause the change of the profiles of nondegenerate bright solitons in the other two components at the same scale. This character is different from the degenerate solitons in the mixed N-coupled nonlinear Schrödinger equations [49], for which the intensity of the bright soliton can increase with decreasing the background amplitude of the dark soliton.

It is well known that the grayness of valley (the background density of dark soliton minus its minimum density) tends to decrease with increasing moving velocity and the symmetric properties do not change for an SVDS. Based on the DVDS solutions Eq. (2), we know that the grayness of each valley is affected by several soliton parameters, such as width-dependent parameters w_j, velocity v_1, and free parameters α_1 and β_2. Particularly, the width-dependent parameters of soliton significantly affect the velocity ranges. For the certain width-dependent parameters w_j, the grayness of DVDS also decreases with increasing moving velocity. However, the multiple exponential functions make the DVDS solution form be much more complicated than the well-known SVDS solution. It is too complicated to quantitatively characterize the influence of other free parameters' on the grayness of each valley. Analysis techniques still need further improvement. Interestingly, the asymmetry degree of two valleys (i.e., the relative grayness) of asymmetric DVDS can vary with velocity. The asymmetry degree is defined as

$$R(v_1) = \frac{I_1 - I_2}{I_1 + I_2}, \tag{3}$$

where I_1 and I_2 are the grayness of the left and right valleys in space, respectively. We exhibit the asymmetry degree vs the moving velocity in Fig. 2 with numerical calculation the grayness of each valley, and keeping the other

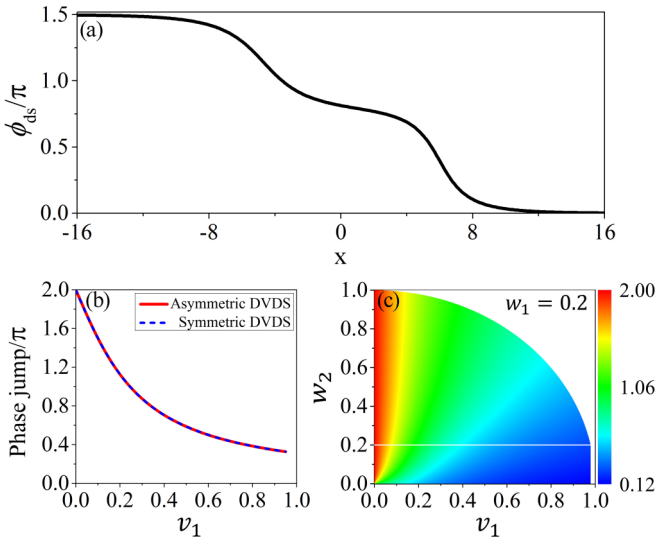

FIG. 3. The phase properties of a DVDS. (a) The phase distribution of an asymmetric DVDS corresponding to the density profile in Fig. 1(a1). We can see that the DVDS admits two phase jumps across two valleys. (b) The phase jump vs moving velocity for DVDSs. The red solid line shows the curve for the asymmetric DVDS, while the blue dashed line shows the curve for the symmetric DVDS. The other parameters for both cases are identical to those in Fig. 1. The phase jump decreases gradually with increasing velocity. (c) The phase jump (in π unit) vs the soliton width-dependent parameter and velocity. The parameter w_1 is fixed at 0.2. This demonstrates that the soliton width-dependent parameters significantly affect the phase jump and velocity region of DVDSs. The other parameters are $\alpha_1 = 0.5$ and $\beta_2 = 0.2$.

parameters be identical with the ones in Fig. 1. The red solid line (blue dashed line) corresponds to the asymmetric (symmetric) DVDS. It is seen that the asymmetry degree crucially depends on the velocity for asymmetric DVDS, whereas $R(v_1)$ is constant for symmetric DVDS. This is also a significant difference between symmetric and asymmetric DVDS.

C. Phase properties of double-valley dark solitons

SVDSs are well known to admit one phase jump across their density dip, which varies in the range $[0, \pi]$ [2,3,20–22]. Generally, the total phase jump of dark soliton can be obtained by calculating the argument $\phi_{ds}(x) = \arg(q_1)$ by dropping the momentum phase of the background. For MVDSs, it should be emphasized that the phase distribution cannot be directly obtained by calculating only the argument of MVDS solutions. We need combine both the argument and the phase gradient flow $\nabla\phi_{ds}(x)$ to properly address the phase variations $\phi_{ds}(x)$ of MVDS [22]. Here, we define the total phase jump as $\triangle\phi_{ds} = \phi_{ds}(x \to -\infty) - \phi_{ds}(x \to +\infty)$. As an example, we plot the corresponding phase distribution of Fig. 1(a1) in Fig. 3(a). Remarkably, the phase variations of DVDS exhibit an apparent two-step structure through two valleys, in contrast to the single-step structure of SVDSs discussed previously [2–5,8,10–17,20–22,31–34,44,47]. Moreover, the total phase jump of a DVDS is larger than π in this case, which is also distinctive from SVDSs (which usually cannot exceed π). We note that SVDSs can admit a phase jump greater than π in a saturable self-defocusing material [50,51] but only one phase jump across the soliton. The phase distribution of a symmetric DVDS is similar to that of an asymmetric DVDS, with only a small difference in the spatial position. Additionally, a bright soliton with one node in component q_2 always maintains a π phase jump, where the abrupt phase change occurs at the node, while a bright soliton without a node has no phase jump in component q_3.

Furthermore, we find that the phase jump of a DVDS changes with the moving velocity. As an example, we display the variation in the phase jump of a DVDS with the velocity in Fig. 3(b), where the red solid line and the blue dashed line represent asymmetric and symmetric DVDSs, respectively. The parameters are the same as in Fig. 1 except for the velocity v_1. The phase jump value decreases dramatically with increasing velocity. For this case, the velocity range is $|v_1| \in [0, \sqrt{91}/10)$, and the phase jump is within the range $[0.32\pi, 2\pi]$. Under the limit of zero velocity, i.e., for a stationary DVDS, the phase jump takes a value of 2π. Figure 3(b) suggests that the change in the phase jump with velocity for a symmetric DVDS is identical to that for an asymmetric DVDS, and the parameters α_1 and β_2 do not affect the phase jump region. However, further analysis indicates that the soliton width-dependent parameters essentially determine the phase jump range. For example, we draw the variation in the phase jump value with the soliton width-dependent parameter w_2 in Fig. 3(c), where w_1 is fixed to be 0.2 herein. With varying w_2, we can calculate the velocity region under the constraint condition $w_j^2 + v_1^2 < 1$. Namely, when $w_2 \in (0, 0.2)$, $|v_1| \in [0, 2\sqrt{6}/5)$; additionally, when $w_2 \in (0.2, 1)$, $|v_1| \in [0, \sqrt{1 - w_2^2})$. Figure 3(c) clearly shows the variation in the phase jump with an increase in the width-dependent parameter w_2, always taking a value of 2π for a static DVDS. With an increase in the width-dependent parameter w_2, the phase jump region decreases since the phase jump value increases at the maximum velocity. With $w_1 = 0.2$, the phase jump range is $[0.12\pi, 2\pi]$. For smaller soliton width-dependent parameters w_1 and w_2, the phase jump value tends to be zero when the soliton's velocity approaches the limit of the maximum velocity, meaning that DVDS admit the largest phase jump range of $[0, 2\pi]$.

We emphasize that the soliton width-dependent parameters also affect the velocity region; as a result, the maximum speed of the DVDS can be much smaller than the speed of sound for DVDS when choosing larger width-dependent parameters [see Fig. 3(c)]. This is a notable characteristic for MVDS that is absent for usual scalar SVDS [20,21]. For usual scalar SVDS, the maximum velocity is the speed of sound. For a bright-dark soliton in a two-component BEC with attractive interactions, the width and velocity are completely independent of each other [47], and there is no limit on the moving velocity. However, for dark-bright solitons in repulsive condensates, a change in the soliton width also causes the velocity range to vary [47]. Our detailed analysis indicates that the relation between the soliton width and velocity satisfies an inequality for MVDS and dark-bright solitons, but this relation becomes an equality for usual scalar SVDS [20,21]. This characteristic of dark-bright solitons has not been taken seriously

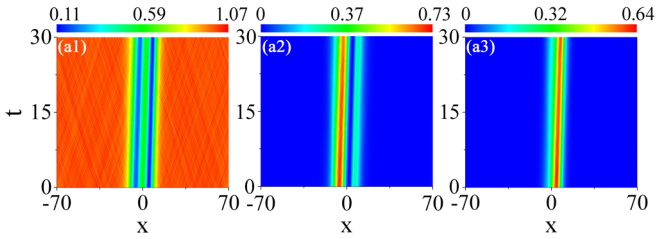

FIG. 4. (a1) The numerical evolution of DVDS when the nonlinear coefficients admit small deviations from Manakov model Eq. (1). The initial excitation condition is given by Eq. (2) at $t = 0$ with adding 2% random noise, and the inter-component nonlinear coefficient is set to be 0.98. The other parameters are the same as in Figs. 1(a1)–1(a3). It is shown that the profile of DVDS remain robust against weak noise and small deviations from the ideal conditions. Panels (a2) and (a3) show the corresponding numerical evolutions of the other two bright soliton components.

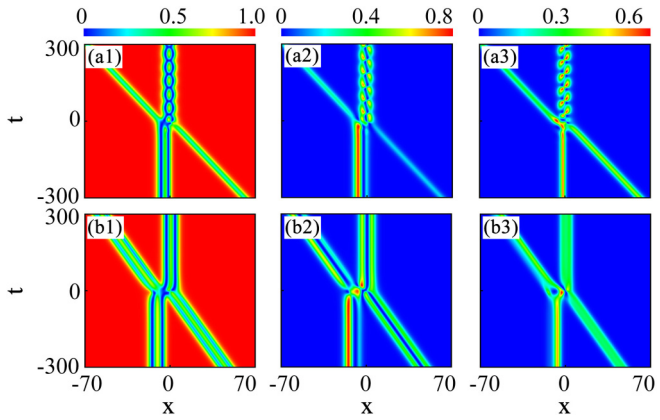

FIG. 5. The collision dynamics of DVDSs. (a1) Collision between one DVDS and an SVDS. There is a striking state transition process in which a DVDS transitions to a breather after the collision, whereas the SVDS does not breath and experiences only slight profile variation. Panels (a2, a3) show similar state transition dynamics in the other bright soliton components. (b1) Collision between two DVDSs. For this case, there is no state transition occurrence for the DVDSs. Panels (b2, b3) display similar collision dynamics in the other bright soliton components. The parameters are $v_1 = 0$, $w_1 = 0.35$, $w_2 = 0.6$, $v_2 = -0.2$, $w_3 = 0.3$, $\alpha_1 = 1$, $\beta_2 = 1$, and $\alpha_3 = \beta_3 = 1$ for panels (a1–a3). The parameters are $v_1 = -0.15$, $w_1 = 0.3$, $w_2 = 0.4$, $v_2 = 0$, $w_3 = 0.35$, $w_4 = 0.45$, $\alpha_1 = 1$, $\beta_2 = 1$, $\alpha_3 = 1$, and $\beta_4 = 1$ for panels (b1–b3).

in previous work [5]. Nevertheless, we expect that the soliton width plays an important role in the motion of dark-bright solitons in harmonic traps, in contrast to the motion of scalar dark solitons in harmonic traps [52]. Therefore, the effects of the soliton width should be considered when discussing the motion of MVDS in external potentials.

D. Stability of double-valley dark solitons

Then, we test the stability of DVDS. The exact DVDS solution Eq. (2a) is derived from the integrable Manakov model, for which the intra- and inter component nonlinear interaction strengths are equal. But these nonlinear interaction strengths can not be equal precisely in real experiments. Therefore, we test the evolutionary stability of DVDS with small deviations from the Manakov model. For example, Fig. 4(a1) exhibits the numerical evolution of DVDS in the model Eq. (1) with setting inter-component nonlinear coefficients to be 0.98 and adding 2% random noises on initial states. Other parameters settings are the same as Figs. 1(a1)–1(a3). Figures 4(a2) and 4(a3) show the corresponding numerical evolutions of the other two bright soliton components. It demonstrates that the profile of DVDS remain stable over a long evolution time. It indicates that it is possible to excite DVDS in experiments with the developed density and phase modulation techniques in ultracold atomic systems [8,15,16,53,54].

Very recently, three-component vector solitons and their collisions were experimentally observed in BECs with repulsive interactions [16]. Motivated by these results, we would like to analytically investigate the collision dynamics of DVDSs by performing further iterations of the developed DT method.

III. COLLISION DYNAMICS OF DOUBLE-VALLEY DARK SOLITONS

The collision dynamics of DVDSs mainly include two cases: (i) a collision between a DVDS and an SVDS, (ii) a collision between two DVDSs. We investigate these two types of collisions based on two dark soliton solutions derived by the threefold and fourfold DT (see details in Appendix A). A collision between two DVDSs usually makes each soliton's profile vary, similar to a collision between nondegenerate bright solitons [24]. However, the collision between a DVDS and an SVDS demonstrates a striking state transition process: The DVDS transforms into a breather after colliding with the SVDS, while the density profile of SVDS do not admit any change after the collision, only with a phase shift.

We first study the interaction between a DVDS and an SVDS based on the exact solution Eq. (A23) by implementing a threefold DT with the introduced complex parameters $\xi_1 = -v_1 + iw_1$, $\xi_2 = -v_1 + iw_2$ (generating a DVDS in component q_1) and $\xi_3 = -v_2 + iw_3$ (generating an SVDS in component q_1) (see Appendix A for the detailed calculation process). A typical example of the striking state transition process is illustrated in Fig. 5(a1). The asymmetric DBBS is evidently transformed into a breather, whose density evolution admits a periodic oscillation behavior. In contrast, the fundamental DBBS (moving toward the left) maintains a soliton state. Such a state transition induced by a collision is not discussed in the previous literatures [4,5,8,20,21]. Figures 5(a2) and 5(a3) show the density evolutions of bright solitons in components q_2 and q_3, respectively, demonstrating that this breathing behavior also emerges after the interaction.

To understand the state transition phenomenon, we further analyze the exact solutions Eq. (A23) through developing the asymptotic analysis technique [27,55,56] with assuming $v_1 > v_2$. Our analysis suggests that the state transition is induced by the mixture of effective energies of the solitons in the three components during the collision process. Before the collision ($t \to -\infty$), the DVDS-related vector soliton solutions take

the following asymptotic forms:

$$q^i_{1,S1} = \frac{f_1 e^{-\nu_1} + f_2 e^{\nu_1} + f_3 e^{-\nu_2} + f_4 e^{\nu_2}}{m_1 e^{-\nu_1} + m_2 e^{\nu_1} + m_3 e^{-\nu_2} + m_4 e^{\nu_2}} e^{-it}, \tag{4a}$$

$$q^i_{2,S1} = \frac{g_1\left(g_2 e^{-\kappa_2} + g_3 e^{\kappa_2}\right)}{m_1 e^{-\nu_1} + m_2 e^{\nu_1} + m_3 e^{-\nu_2} + m_4 e^{\nu_2}} e^{i\varphi_1}, \tag{4b}$$

$$q^i_{3,S1} = \frac{h_1\left(h_2 e^{-\kappa_1} - h_3 e^{\kappa_1}\right)}{m_1 e^{-\nu_1} + m_2 e^{\nu_1} + m_3 e^{-\nu_2} + m_4 e^{\nu_2}} e^{i\varphi_2}, \tag{4c}$$

where $\kappa_j = w_j(x - v_1 t)$, $\varphi_j = v_1 x - \frac{1}{2}(v_1^2 - w_j^2 + 2)t$, $\nu_1 = \kappa_1 + \kappa_2$ and $\nu_2 = \kappa_1 - \kappa_2$ $(j = 1, 2)$. The expressions for f_i, g_i, h_i and m_i are given in Appendix B, and they are all complex constants. After the collision ($t \to +\infty$), the asymptotic analysis expressions for the vector breather take the following forms:

$$q^f_{1,S1} = \frac{(\delta_1 e^{-i\theta} + \delta_2 e^{i\theta} + \delta_3 e^{-\nu_1} + \delta_4 e^{\nu_1} + \delta_5 e^{\nu_2} + \delta_6 e^{-\nu_2}) e^{-it}}{\varrho_1(\varrho_2 e^{-i\theta} + \varrho_2^* e^{i\theta}) + \varrho_3 e^{-\nu_1} + \varrho_4 e^{\nu_1} + \varrho_5 e^{\nu_2} + \varrho_6 e^{-\nu_2}}, \tag{5a}$$

$$q^f_{2,S1} = \frac{i4\lambda_1^i e^{i\varphi_1}(\rho_1 e^{-\kappa_2} + \rho_2 e^{\kappa_2}) + i4\lambda_2^i e^{i\varphi_2}(\rho_3 e^{-\kappa_1} + \rho_4 e^{\kappa_1})}{\varrho_1(\varrho_2 e^{-i\theta} + \varrho_2^* e^{i\theta}) + \varrho_3 e^{-\nu_1} + \varrho_4 e^{\nu_1} + \varrho_5 e^{\nu_2} + \varrho_6 e^{-\nu_2}}, \tag{5b}$$

$$q^f_{3,S1} = \frac{i4\lambda_1^i e^{i\varphi_1}(\vartheta_1 e^{-\kappa_2} + \vartheta_2 e^{\kappa_2}) + i4\lambda_2^i e^{i\varphi_2}(\vartheta_3 e^{-\kappa_1} + \vartheta_4 e^{\kappa_1})}{\varrho_1(\varrho_2 e^{-i\theta} + \varrho_2^* e^{i\theta}) + \varrho_3 e^{-\nu_1} + \varrho_4 e^{\nu_1} + \varrho_5 e^{\nu_2} + \varrho_6 e^{-\nu_2}}, \tag{5c}$$

where $\theta = \varphi_1 - \varphi_2 = \frac{1}{2}(w_1^2 - w_2^2)t$. The expressions for δ_i, ρ_i, ϑ_i, and ϱ_i are presented in Appendix B, and they are all complex constants. λ_1^i and λ_2^i correspond to the imaginary part of the spectral parameters λ_1 and λ_2, respectively. The symbol "*" denotes complex conjugate. From Eq. (4), we can see that each initial soliton admits a certain velocity. As shown in Ref. [22], a moving soliton solution can be transformed to an eigenstate with an eigenenergy if we choose the soliton center as a frame of reference. Therefore, it is reasonable to define an effective energy for the solitons as $E_j^* = \frac{d\phi_j}{dt}$ (where ϕ_j is the phase of the wave function). We know that the effective energy of the soliton in components q_1, q_2, and q_3 is $E_1^* = -1$, $E_2^* = -\frac{1}{2}(v_1^2 - w_1^2 + 2)$, and $E_3^* = -\frac{1}{2}(v_1^2 - w_2^2 + 2)$, respectively. From Eq. (5), we can see that the effective energies of bright soliton components mix and emerge in the DVDS component after the collision process. The breathing behavior obviously originates from the energy mixing term in $e^{\pm i\theta}$. Namely, the effective energy difference of bright solitons determines the oscillation period, and the period is

$$T = \frac{2\pi}{|E_2^* - E_3^*|} = \frac{4\pi}{|w_1^2 - w_2^2|}. \tag{6}$$

The oscillation period is identical among the three components. Based on this discussion, we also revisit the collision dynamics of nondegenerate bright solitons [24] and find that an effective energy mixture can also emerge. This means that the above-mentioned breather behavior is also observable during the collision between a nondegenerate bright soliton and a degenerate bright soliton.

To make a comprehensive analysis of this state transition phenomenon, we also present the asymptotic expressions of the fundamental DBBS before and after collision to discuss its collision properties. Before the collision ($t \to -\infty$), the solution for the fundamental DBBS is derived as follows:

$$q^i_{1,S2} = \left[-\frac{v_2}{\xi_3} + i\frac{w_3}{\xi_3}\tanh(\kappa_3 + d_1)\right] e^{-it}, \tag{7a}$$

$$q^i_{2,S2} = \frac{\alpha_3 \xi_1^* \eta_{13} r_3}{2\xi_1 \xi_3 \varpi_{31}\sqrt{x_1}} \operatorname{sech}(\kappa_3 + d_1) e^{i\varphi_3}, \tag{7b}$$

$$q^i_{3,S2} = \frac{\beta_3 \xi_2^* \eta_{23} r_3}{2\xi_2 \xi_3 \varpi_{32}\sqrt{x_1}} \operatorname{sech}(\kappa_3 + d_1) e^{i\varphi_3}, \tag{7c}$$

Here, $\kappa_3 = w_3(x - v_2 t)$, $\varphi_3 = v_2 x - \frac{1}{2}(v_2^2 - w_3^2 + 2)t$. The explicit expressions of ϖ_{ij}, η_{ij}, r_i, x_1 and d_1 are given in Appendix B, and they are all complex constants. Based on the Eq. (7), we can get the grayness (G^i) of valley of SVDS in the component q_1, peak value (P_1^i) of bright soliton in the component q_2 and peak value (P_2^i) of bright soliton in the component q_3 before the collision. They can be calculated as $G^i = \frac{w_3^2}{v_2^2 + w_3^2}$, $P_1^i = \frac{\alpha_3^2 |\varpi_{23}|^2 |\eta_{13}|^2 r_3^2}{4|\xi_3|^2(\alpha_3^2|\varpi_{23}|^2|\eta_{13}|^2 + \beta_3^2|\varpi_{13}|^2|\eta_{23}|^2)}$ and $P_2^i = \frac{\beta_3^2 |\varpi_{13}|^2 |\eta_{23}|^2 r_3^2}{4|\xi_3|^2(\alpha_3^2|\varpi_{23}|^2|\eta_{13}|^2 + \beta_3^2|\varpi_{13}|^2|\eta_{23}|^2)}$. After the collision ($t \to +\infty$), the fundamental DBBS is give by

$$q^f_{1,S2} = \frac{\xi_1^* \xi_2^*}{\xi_1 \xi_2}\left[-\frac{v_2}{\xi_3} + i\frac{w_3}{\xi_3}\tanh(\kappa_3 + d_2)\right] e^{-it}, \tag{8a}$$

$$q^f_{2,S2} = \frac{\alpha_3 z_{13} z_{32}^* r_3}{2\xi_3 y_{31} y_{32}\sqrt{x_2}} \operatorname{sech}(\kappa_3 + d_2) e^{i\varphi_3}, \tag{8b}$$

$$q^f_{3,S2} = \frac{\beta_3 z_{13} z_{32}^* r_3}{2\xi_3 y_{31} y_{32}\sqrt{x_2}} \operatorname{sech}(\kappa_3 + d_2) e^{i\varphi_3}. \tag{8c}$$

The explicit expressions of z_{ij}, y_{ij}, x_2, and d_2 are given in Appendix B, and they are all complex constants. With using the asymptotic analysis results Eq. (8), we can also obtain grayness (G^i) of valley of SVDS in the component q_1, peak value (P_1^f) of bright soliton in the component q_2 and peak value (P_2^f) of bright soliton in the component q_3 after

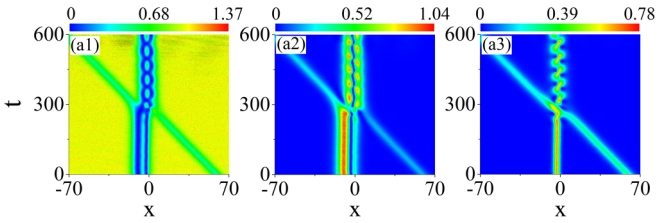

FIG. 6. (a1) The numerical evolution of the collision between one DVDS and one SVDS. Panels (a2) and (a3) correspond to the other two bright soliton components. The initial excitation condition are the same as in Figs. 5(a1)–5(a3) at $t = -300$ with adding 5% random noise in each component. It is seen the state transitions between DVDS and breather state are robust against weak noise.

the collision. They can be calculated as $G^f = \frac{w_3^2}{v_2^2+w_3^2}$, $P_1^f = \frac{\alpha_3^2|r_3|^2}{4|\xi_3|^2(\alpha_3^2+\beta_3^2)}$, and $P_2^f = \frac{\beta_3^2|r_3|^2}{4|\xi_3|^2(\alpha_3^2+\beta_3^2)}$.

Based on the asymptotic expressions Eqs. (7) and (8), we can analyze the change of fundamental DBBS's density profile during the breathing state transition. Particularly, Eqs. (7a) and (8a) indicate that the density profile of SVDS remain unchanged after the occurrence of breathing states. The grayness of valley keep the same ($G^i = G^f$). However, there are significant alterations of density profiles for degenerate bright solitons in the other two components ($P_1^i \neq P_1^f$ and $P_2^i \neq P_2^f$), based on the asymptotic expressions Eqs. (7b), (7c) and (8b), (8c). This means that population redistribution happens between single-hump bright soliton and asymmetric double-hump bright soliton during their collision process in the component q_2. Similar phenomenon also emerges in the component q_3. In addition, our numerical simulation indicates that the striking breathing state transition is robust against weak noises. For instance, the numerical results are depicted in Fig. 6, for which the initial excitation form is given by the exact ones at $t = -300$ in Figs. 5(a1)–5(a3) with adding 5% white noise. This partly means that state transition between a DVDS and a breather obtained here could be observed in a real condensate system.

Next, we investigate the interaction between two DVDSs based on the exact solutions Eq. (A24) by implementing a fourfold DT with the parameters $\xi_1 = -v_1 + iw_1$, $\xi_2 = -v_1 + iw_2$ (which generates one DVDS), $\xi_3 = -v_2 + iw_3$, and $\xi_4 = -v_2 + iw_4$ (which generates another DVDS) (see Appendix A for the detailed calculation process). For this case, a typical example of the density distribution is displayed in the second panel of Fig. 5, for which Figs. 5(b1), 5(b2), and 5(b3) correspond to component q_1, component q_2, and component q_3, respectively. As shown in Fig. 5(b1), the collision between the two DVDSs causes their profiles to change, accompanied by a phase shift. However, for this case, there is no state transition occurrence for either DVDS, which is dramatically different from the collision dynamics between the DVDS and SVDS described in Fig. 5(a1). Moreover, the effective energy mixture no longer emerges in this case. The inelastic collision dynamics for the other two bright soliton components [see Figs. 5(b2) and 5(b3)] are similar to the those for the two nondegenerate bright solitons that collide in Ref. [24]. Additionally, the numerical simulations also demonstrates that interaction between two DVDSs are also robust against small noise, we do not show them herein.

IV. TRIPLE-VALLEY DARK SOLITONS IN FOUR-COMPONENT REPULSIVE CONDENSATES

We now extend our discussion to four-component BECs with repulsive interactions, which are described by the following repulsive four-component Manakov model:

$$iq_{j,t} + \tfrac{1}{2}q_{j,xx} - (|q_1|^2 + |q_2|^2 + |q_3|^2 + |q_4|^2)q_j = 0, \quad (9)$$

where $q_j(x,t)(j = 1,2,3,4)$ denote the four component fields in BECs. By applying the threefold DT with $\lambda_j = 1/2(\xi_j + 1/\xi_j)$ and $\xi_j = -v_1 + iw_j$ $(j = 1,2,3)$, which is similar to the DT presented in Appendix A, we can obtain a new class of dark-bright-bright-bright soliton solutions, which admits a TVDS in component q_1 and triple-hump bright solitons in the other three components. The exact soliton solutions can be expressed in the following form:

$$q_1 = \frac{1}{\xi_1\xi_2\xi_3}\frac{N_1}{M_1}e^{-it}, \quad (10a)$$

$$q_2 = -i\frac{2w_1}{\xi_1}\alpha\sqrt{1-v_1^2-w_1^2}\frac{N_2}{M_1}e^{i[v_1x-\frac{1}{2}(2+v_1^2-w_1^2)t]}, \quad (10b)$$

$$q_3 = -i\frac{2w_2}{\xi_2}\beta\sqrt{1-v_1^2-w_2^2}\frac{N_3}{M_1}e^{i[v_1x-\frac{1}{2}(2+v_1^2-w_2^2)t]}, \quad (10c)$$

$$q_4 = -i\frac{2w_3}{\xi_3}\gamma\sqrt{1-v_1^2-w_3^2}\frac{N_4}{M_1}e^{i[v_1x-\frac{1}{2}(2+v_1^2-w_3^2)t]}, \quad (10d)$$

with

$$\kappa_1 = 2w_1(x - v_1t), \kappa_2 = 2w_2(x - v_1t), \kappa_3 = 2w_3(x - v_1t),$$

$$N_1 = \xi_1\xi_2^*\xi_3^*\alpha^2\eta_2e^{\kappa_1} + \xi_1^*\xi_2\xi_3^*\beta^2\eta_3e^{\kappa_2} + \xi_1^*\xi_2^*\xi_3\gamma^2\eta_4e^{\kappa_3} + \eta_5\big[\xi_1\xi_2\xi_3\alpha^2\beta^2\gamma^2e^{\kappa_1+\kappa_2+\kappa_3} + \xi_1^*\xi_2\xi_3\beta^2\gamma^2e^{\kappa_2+\kappa_3} + \xi_1\xi_2\xi_3^*\alpha^3\beta^2e^{\kappa_1+\kappa_2} + \xi_1\xi_2^*\xi_3\alpha^2\gamma^2e^{\kappa_1+\kappa_3}\big] + \xi_1^*\xi_2^*\xi_3^*\eta_1,$$

$$N_2 = \big[p_1 + p_2\beta^2e^{\kappa_2} + p_3\gamma^2e^{\kappa_3} + \eta_5\beta^2\gamma^2e^{\kappa_2+\kappa_3}\big]e^{\kappa_1/2},$$

$$N_3 = \big[p_4 + p_5\alpha^2e^{\kappa_1} - p_3\gamma^2e^{\kappa_3} + \eta_5\alpha^2\gamma^2e^{\kappa_1+\kappa_3}\big]e^{\kappa_2/2},$$

$$N_4 = \big[p_6 - p_5\alpha^2e^{\kappa_1} - p_2\beta^2e^{\kappa_3} + \eta_5\alpha^2\beta^2e^{\kappa_1+\kappa_2}\big]e^{\kappa_3/2},$$

$$M_1 = \big[\alpha^2\beta^2e^{\kappa_1+\kappa_2} + \alpha^2\gamma^2e^{\kappa_1+\kappa_3} + \beta^2\gamma^2e^{\kappa_2+\kappa_3}\big]\eta_5 + \eta_1 + \eta_2\alpha^2e^{\kappa_1} + \eta_3\beta^2e^{\kappa_2} + \eta_4\gamma^2e^{\kappa_3} + \eta_5\alpha^2\beta^2\gamma^2e^{\kappa_1+\kappa_2+\kappa_3}.$$

The expressions η_i and p_i are shown in Appendix C. The parameters v_1, w_1, w_2, w_3, α, β, and γ are real constants that codetermine the profile and position of the TVDS. The parameters w_1, w_2, and w_3 are three width-dependent parameters of soliton($w_1 \neq w_2 \neq w_3$). The parameter v_1 is the soliton velocity, which should satisfy the constraint $v_1^2 + w_j^2 < 1$ $(j = 1,2,3)$. The parameters α, β, and γ are three free parameters associated with the center positions and relative values of the three valleys. The profile of the TVDS is generally asymmetric but becomes symmetric for certain values of the parameters α, β, and γ, which is similar to the above three-component case. With the arbitrary setting of these parameters, the solution given in Eq. (10) shows a TVDS in component q_1, a triple-hump bright soliton with two nodes in component q_2, a bright soliton with one node in component

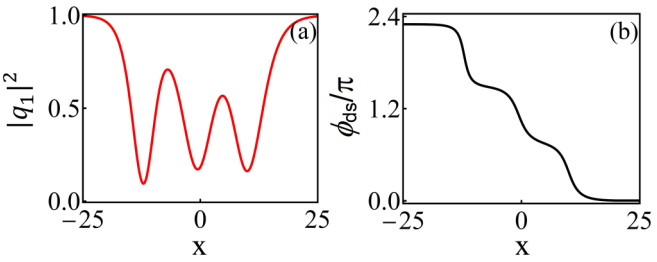

FIG. 7. The density profile (a) and phase distribution (b) of an asymmetric TVDS. Three phase jumps across the three density valleys can be observed. The parameters are $v_1 = 0.1$, $w_1 = 0.2$, $w_2 = 0.28$, $w_3 = 0.33$, $\alpha = \frac{1}{6}$, $\beta = \frac{1}{10}$, $\gamma = 1$.

q_3 and a bright soliton without a node in component q_4. The density profiles of multihump bright solitons in the last three components are similar to the solitons reported in three component attractive BECs [24]. In this section, we mainly discuss the TVDS in the first component.

The density profile of an asymmetric TVDS are displayed in Fig. 7(a). Our numerical simulations show that TVDS is also robust against small nonlinear coefficients deviations and weak noise, similar to DVDS exhibited in Fig. 4(a1). So we do not show them again here. The structure of TVDS is somewhat similar to those of stationary multisoliton complexes on a background [57,58], both are formed as the special nonlinear superpositions of pairs of bright and dark solitons. But there are still some differences between our TVDS solution and the ones in Refs. [57,58]. First, we develop DT method to derive the solution directly, in contrast to the sophisticated rotation transformation in Ref. [57] or the nonlinear superposition of a radiation modes in Ref. [58] based on the bright multisoliton complexs. This makes the soliton solution's expressions be quite different. The explicit relations between them still need further studies. Moreover, the collision dynamics of TVDSs include three main cases: a collision between a TVDS and an SVDS, a collision between a TVDS and a DVDS, and a collision between two TVDSs. A breather transition also emerges for the TVDS in the first and second cases, while the soliton profiles vary after the collision without breather behavior in the third case. The state transition behaviors have not been discussed in Refs. [57,58].

We also present the corresponding phase distribution of TVDS in Fig. 7(b). It demonstrates that the TVDS features three phase jumps across three valleys. The soliton width-dependent parameter w_j also affects the phase jump region of the TVDS. As an example, we demonstrate the variation in the phase jump value with the changes in the soliton width-dependent parameters (w_2 and w_3) and the velocity in Fig. 8. The parameter w_1 is fixed to be 0.2. For the static TVDS solution, the phase jump is 3π. The phase jump value achieves the minimum value when the velocity tends toward the limit of the maximum velocity. With $w_1 = 0.2$, the phase jump range of the TVDS is $[0.14\pi, 3\pi]$, but the phase jump range of the TVDS can vary within $[0, 3\pi]$ by further decreasing the value of w_1. The phase jumps of triple-hump bright solitons in component q_2, component q_3, and component q_4 are always 2π, π and 0, respectively. Moreover, the parameters w_j can also vary the soliton velocity region for a TVDS. The velocity

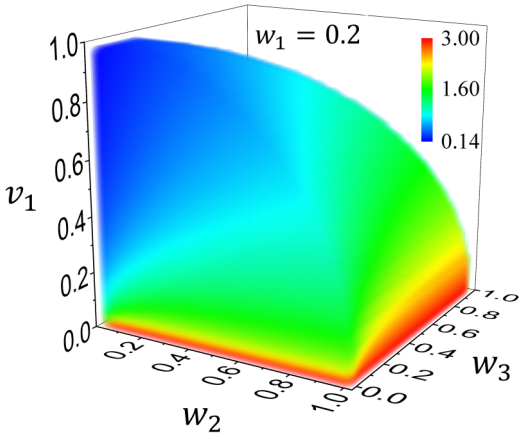

FIG. 8. The phase jump (in π unit) of a TVDS with varying velocity and soliton width-dependent parameters w_2 and w_3. The width-dependent parameters significantly affect the phase jump and velocity region. w_1 is fixed to be 0.2. The other parameters are $\alpha = 1/6$, $\beta = 1/10$, $\gamma = 1$.

range is $[0, \sqrt{1 - w_m^2})$, where w_m is the largest of the three width-dependent parameters. These characteristics are similar to those of the DVDS case, which could hold for dark solitons with more valleys.

V. CONCLUSION AND DISCUSSION

We obtain exact DVDS and TVDS solutions by further developing the DT method. Their velocity and phase jump characteristics are characterized in detail. In particular, we demonstrate that changes in the soliton width-dependent parameters have considerable influences on the velocity and phase jump ranges. This finding indicates that the effects of the soliton width should be considered when studying the motion of MVDSs in external potentials. The collision dynamics of the DVDS and TVDS are also discussed. The collisions involving DVDSs are discussed in detail, and we report a striking state transition process in which a DVDS turns into a breather after colliding with an SVDS due to the mixture of the effective energies of the soliton states in the three components. Furthermore, our analyses suggest that breather transitions exist widely in the collision processes involving MVDSs.

Very recently, nondegenerate bright solitons were discussed in a N-component coupled systems with attractive interactions [59], based Hirota bilinear method. Our discussion can also be extended to N-component coupled systems with repulsive interactions. The $(N-1)$-valley dark soliton solution can be obtained by applying the $(N-1)$-fold DT with similar constraint conditions on the eigenfunctions of the Lax pair. The phase jump of the $(N-1)$-valley dark soliton could vary in the region $[0, (N-1)\pi]$. This argument is supported by our calculation up to a five-component case. Nevertheless, further study is needed to learn how to express the analytical solution for arbitrary N-component coupled systems. The collision properties between MVDSs and degenerate vector solitons are expected to be much more abundant than those of previously reported vector soliton collisions

[5,16,36,43,47]. In particular, the state transition between the breather and MVDS could have some important hints for soliton state manipulation fields.

Recently, three-component vector solitons and their collisions were experimentally observed in BECs with repulsive interactions [16]. This finding indicates that soliton dynamics could be quantitatively described by the above integrable repulsive three-component Manakov model. Therefore, we discuss the possibilities to observe DVDSs in three-component repulsive BECs in combination with well-developed quantum engineering techniques [8,15,16,53,54]. In this repulsive interaction case, the DVDS should be prepared firstly and then it creates an effective potential, which is essential for double-hump bright solitons generation in the other components. Now, let us consider quasi-one-dimensional elongated BECs of ^{87}Rb. The different components are the magnetic sublevels $m_F = 0, \pm 1$ of the $F = 1$ hyperfine manifold. In the beginning, all atoms are prepared in the $m_F = 0$ state. One can use spatial local control beams to transfer atoms from the initial state $m_F = 0$ to $m_F = \pm 1$ [16]. With knowledge of the density and phase given by the solution of Eq. (2), one could transfer the atom and imprint phase on them simultaneously to approach the initial state for the DVDS and bright soliton states in the corresponding components. Moreover, our numerical simulations show that these soliton states are robust against small deviations and weak noises (see Fig. 4). Therefore, there are many possibilities to observe them in real experiments.

ACKNOWLEDGMENTS

This work is supported by the National Natural Science Foundation of China (Contracts No. 12022513, No. 11775176, and No. 12047502), the Major Basic Research Program of Natural Science of Shaanxi Province (Grant No. 2018KJXX-094), Scientific research program of Education Department of Shaanxi Provience (Grant No. 18JK0098), and Scientific Research Foundation of SUST (Grant No. 2017BJ-30). L.L. acknowledges support from the National Natural Science Foundation of China (Grant No. 11771151), the Guangzhou Science and Technology Program of China (Grant No. 201904010362), and the Fundamental Research Funds for the Central Universities of China (Grant No. 2019MS110)

APPENDIX A: DERIVATION OF THE DOUBLE-VALLEY DARK SOLITON SOLUTION OF EQUATION (1)

The N-component repulsive BEC can be described by the following N-coupled Manakov model [16,44]:

$$i\mathbf{q}_t + \tfrac{1}{2}\mathbf{q}_{xx} - \mathbf{q}^\dagger\mathbf{q}\mathbf{q} = 0, \tag{A1}$$

where

$$\mathbf{q} = (q_1, q_2, \ldots q_N)^\mathsf{T},$$

which admits the following Lax pair:

$$\psi_x = U(\lambda; Q)\psi, \tag{A2a}$$

$$\psi_t = V(\lambda; Q)\psi, \tag{A2b}$$

with

$$U = (i\lambda\sigma_3 + iQ), \tag{A3a}$$

$$V = \left[i\lambda^2\sigma_3 + i\lambda Q - \tfrac{1}{2}(i\sigma_3 Q^2 - \sigma_3 Q_x)\right], \tag{A3b}$$

where

$$Q = \begin{bmatrix} 0 & -\mathbf{q}^\dagger \\ \mathbf{q} & \mathbf{0}_{N\times N} \end{bmatrix}, \quad \sigma_3 = \begin{bmatrix} 1 & \mathbf{0}_{1\times N} \\ \mathbf{0}_{N\times 1} & -\mathbb{I}_{N\times N} \end{bmatrix}.$$

As mentioned in the main text, multivalley dark solitons can be obtained in an $N(N > 2)$ component system. As an example, we will take the DVDS solution derivation process in the three-component case to introduce the calculation method for MVDSs.

To obtain the DVDS solutions, we use the following seed solutions:

$$q_{01} = e^{-it}, \quad q_{02} = 0, q_{03} = 0. \tag{A4}$$

First, we need to solve the Lax pair Eq. (A2) with the above seed solutions. We use the following gauge transformation:

$$S = \mathrm{diag}(1, e^{it}, 1, 1),$$

which converts the variable coefficient differential equation into a constant-coefficient equation. Then, we can obtain

$$\psi_{0,x} = U_0\psi_0, \tag{A5a}$$

$$\psi_{0,t} = \left(\frac{\mathrm{i}}{2}U_0^2 + \lambda U_0 + \frac{\mathrm{i}}{2}\lambda^2\right)\psi_0, \tag{A5b}$$

where

$$U_0 = i\begin{bmatrix} \lambda & -1 & 0 & 0 \\ 1 & -\lambda & 0 & 0 \\ 0 & 0 & -\lambda & 0 \\ 0 & 0 & 0 & -\lambda \end{bmatrix}.$$

In the following, we consider the property of U_0. We can obtain the characteristic equation of matrix U_0 at $\lambda = \lambda_j = a_j + ib_j$:

$$\det(i\tau_j - U_0) = (\lambda_j + \tau_j)^2\left(\tau_j^2 - \lambda_j^2 + 1\right) = 0. \tag{A6}$$

The eigenvalues of Eq. (A6) are

$$\tau_{j1} = -\sqrt{\lambda_j^2 - 1}, \tau_{j2} = \tau_{j3} = -\lambda_j, \tau_{j4} = \sqrt{\lambda_j^2 - 1}. \tag{A7}$$

To obtain the vector solution of Eq. (A2), we further diagonalize the matrix U_0. Then, we obtain

$$\phi_x = \widetilde{U}_0\phi, \quad \phi = H^{-1}S\psi, \tag{A8a}$$

$$\phi_t = \left(\frac{i}{2}\widetilde{U}_0^2 + \lambda_j\widetilde{U}_0 + \frac{i}{2}\lambda_j^2\right)\phi, \tag{A8b}$$

where the transformation matrix H can be expressed as the following form:

$$H = \begin{pmatrix} \lambda_j + 1 + \tau_{j1} & 0 & 0 & \lambda_j + 1 + \tau_{j4} \\ \lambda_j + 1 - \tau_{j1} & 0 & 0 & \lambda_j + 1 - \tau_{j4} \\ 0 & 1 & 0 & 0 \\ 0 & 0 & 1 & 0 \end{pmatrix}.$$

Thus, we have the vector solution for Eq. (A8):

$$\phi_j = \begin{pmatrix} \phi_{j1} \\ \phi_{j2} \\ \phi_{j3} \\ \phi_{j4} \end{pmatrix} = \begin{pmatrix} c_{j1} \exp i\left[\tau_{j1}x + \frac{1}{2}\left(\lambda_j^2 + 2\lambda\tau_{j1} - \tau_{j1}^2\right)t\right] \\ c_{j2} \exp i\left[\tau_{j2}x + \frac{1}{2}\left(\lambda_j^2 + 2\lambda\tau_{j2} - \tau_{j2}^2\right)t\right] \\ c_{j3} \exp i\left[\tau_{j3}x + \frac{1}{2}\left(\lambda_j^2 + 2\lambda\tau_{j3} - \tau_{j3}^2\right)t\right] \\ c_{j4} \exp i\left[\tau_{j4}x + \frac{1}{2}\left(\lambda_j^2 + 2\lambda\tau_{j4} - \tau_{j4}^2\right)t\right] \end{pmatrix}. \tag{A9}$$

The coefficients c_{j1}, c_{j2}, c_{j3}, and c_{j4} are arbitrary complex parameters. Then, the special solution of Lax pair Eq. (A2) at λ_j can be obtained based on $\psi_j = S^{-1}H\phi_j$:

$$\begin{aligned} \psi_j &= \begin{pmatrix} \psi_{j1} \\ \psi_{j2} \\ \psi_{j3} \\ \psi_{j4} \end{pmatrix} \\ &= \begin{pmatrix} (1+\lambda+\tau_{j1})\phi_{j1} + (1+\lambda+\tau_{j4})\phi_{j4} \\ [(1+\lambda-\tau_{j1})\phi_{j1} + (1+\lambda-\tau_{j4})\phi_{j4}]e^{-it} \\ \phi_{j2} \\ \phi_{j3} \end{pmatrix}. \end{aligned} \tag{A10}$$

We can see from Eq. (A7) that the algebraic Eq. (A6) has a pair of opposite complex roots, i.e., $\tau_{j1} = -\tau_{j4}$. To obtain the DVDS, we pick only one of them in special solution Eq. (A10). Namely, we need to let $\phi_{j1} = 0$ (i.e., the coefficient $c_{j1} = 0$) or $\phi_{j4} = 0$ (i.e., the coefficient $c_{j4} = 0$). In this paper, we choose $\phi_{j4} = 0$. Then, the above special solutions ψ_j for spectral problem Eq. (A2) at λ_j are re-expressed as follows:

$$\psi_j = \begin{pmatrix} \psi_{j1} \\ \psi_{j2} \\ \psi_{j3} \\ \psi_{j4} \end{pmatrix} = \begin{pmatrix} (1+\lambda+\tau_{j1})\phi_{j1} \\ [(1+\lambda-\tau_{j1})\phi_{j1}]e^{-it} \\ \phi_{j2} \\ \phi_{j3} \end{pmatrix}. \tag{A11}$$

Next, we need to perform a twofold DT using the special solutions Eq. (A11) to derive the DVDS solutions. First, we perform the first-step iteration by applying the DT in Ref. [44] with $\lambda_1 = a_1 + ib_1$ and constrain the eigenfunction $\psi_{13} = \phi_{12} = 0$, i.e., the coefficient $c_{12} = 0$ (or the eigenfunction $\psi_{14} = \phi_{13} = 0$, i.e., the coefficient $c_{13} = 0$):

$$\begin{aligned} &\psi[1] = T[1]\psi, \quad T[1] = \mathbb{I} + \frac{\lambda_1^* - \lambda_1}{\lambda - \lambda_1^*}\frac{\psi_1\psi_1^\dagger\Lambda}{\psi_1^\dagger\Lambda\psi_1}, \\ &Q[1] = Q + (\lambda_1 - \lambda_1^*)\left[\sigma_3, \frac{\psi_1\psi_1^\dagger\Lambda}{\psi_1^\dagger\Lambda\psi_1}\right], \end{aligned} \tag{A12}$$

where $\Lambda = \mathrm{diag}(1,-1,-1,-1)$ and a dagger denotes the matrix transpose and complex conjugate. For the second-step iteration, we employ ψ_2, which is mapped to $\psi_2[1] = T[1]|_{\lambda=\lambda_2}\psi_2$ with $\lambda_2 = a_2 + ib_2$, and we constrain the eigenfunction $\psi_{24} = \phi_{23} = 0$, i.e., the coefficient $c_{23} = 0$ (or the eigenfunction $\psi_{23} = \phi_{22} = 0$, i.e., the coefficient $c_{22} = 0$):

$$\begin{aligned} &\psi[2] = T[2]\psi[1], T[2] = \mathbb{I} + \frac{\lambda_2^* - \lambda_2}{\lambda - \lambda_2^*}\frac{\psi_2[1]\psi_2[1]^\dagger\Lambda}{\psi_2[1]^\dagger\Lambda\psi_2[1]}, \\ &Q[2] = Q[1] + (\lambda_2 - \lambda_2^*)\left[\sigma_3, \frac{\psi_2[1]\psi_2[1]^\dagger\Lambda}{\psi_2[1]^\dagger\Lambda\psi_2[1]}\right]. \end{aligned} \tag{A13}$$

Now, the solution Eq. (A13) will describe the incoherent interaction of incoherent solitons. Based on the generation mechanism of nondegenerate solitons [24], it requires the velocity of incoherent soliton to be equal. Only if the above iterative processes and velocity requirements are met can the first component of solution $Q[2]$ be the DVDS solution. Then, we need to analyze the relationship between the soliton velocity and spectral parameter λ_j.

We find that the solitons' velocities can be obtained by calculating the following:

$$\widetilde{v}_j = \frac{[\mathrm{Im}(\tau_{j1}) - b_j]\mathrm{Re}(\tau_{j1}) - [\mathrm{Im}(\tau_{j1}) + 3b_j]a_j}{\mathrm{Im}(\tau_{j1}) + b_j}, \tag{A14}$$

and the inverse soliton width is

$$\widetilde{w}_j = -[\mathrm{Im}(\tau_{j1}) + b_j]. \tag{A15}$$

Moreover, the spectral parameters should satisfy the constraint condition

$$[b_j - \mathrm{Im}(\tau_{j1})]^2 + [a_j - \mathrm{Re}(\tau_{j1})]^2 - 1 > 0. \tag{A16}$$

With the spectral parameter $\lambda_j = a_j + ib_j$, the velocity or width of the soliton cannot be directly determined by the real or imaginary part of the spectral parameter. This greatly increases the difficulty of taking the equal velocity in the twofold DT Eqs. (A12) and (A13) with different spectral parameters. Accordingly, we express the real and imaginary parts of the spectrum parameter by the velocity $\widetilde{v}_j$ and width $\widetilde{w}_j$. By combining Eqs. (A14)–(A16) and performing further calculations, we obtain

$$a_j = -\frac{\widetilde{v}_j\left(1 + \widetilde{v}_j^2 + \widetilde{w}_j^2\right)}{2\left(\widetilde{v}_j^2 + \widetilde{w}_j^2\right)}, \quad b_j = \frac{\widetilde{w}_j\left(1 - \widetilde{v}_j^2 - \widetilde{w}_j^2\right)}{2\left(\widetilde{v}_j^2 + \widetilde{w}_j^2\right)}, \tag{A17}$$

and the constrain condition is represented as

$$\widetilde{v}_j^2 + \widetilde{w}_j^2 < 1. \tag{A18}$$

Under this representation, one can guarantee that the solitons' velocities in the first-step iteration Eq. (A12) and the second-step iteration Eq. (A13) remain exactly equal, i.e., $\widetilde{v}_2 = \widetilde{v}_1$. In other words, by performing the iterations in Eqs. (A12) and (A13) and setting the spectral parameters under the condition Eqs. (A17) and (A18), the first component of $Q[2]$ is the DVDS solution.

As we have mentioned above, the velocity expression plays a crucial role in the derivation process of multivalley dark solitons. However, for the spectral parameter with the form $\lambda_j = a_j + ib_j$, we must take the square root of a complex number to obtain the physical parameters, namely, the velocity and width. To facilitate this analysis, we employ a more direct approach. Interestingly, we note that if we describe the spectral parameter with the form $\lambda_j = \frac{1}{2}(\xi_j + \frac{1}{\xi_j})$ with an arbitrary complex parameter $\xi_j = -v_j + iw_j$, the solution can be simplified greatly. For this case, v_j of real part is velocity, and imaginary part w_j is the width-dependent parameter of soliton. The physical meanings of the parameters v_j and w_j are much clearer than those of the parameters a_j and b_j [compared to Eq. (A17)], as shown in Fig. 9. Then the eigenvalues

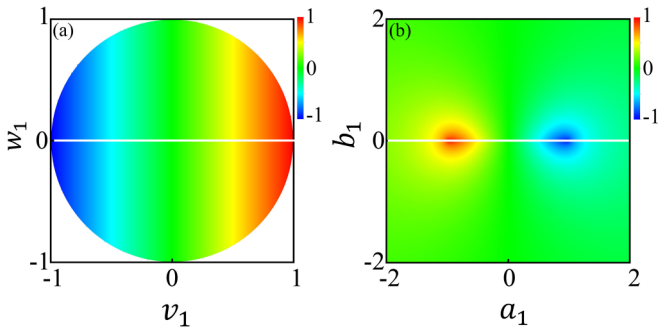

FIG. 9. The relation between the velocity and spectral parameter expressed by different representations. (a) The spectral parameter is written as $\lambda_1 = \frac{1}{2}(\xi_1 + 1/\xi_1)$ with $\xi_1 = -v_1 + iw_1$. For this case, v_1 is the velocity of the soliton. Therefore, there is a linear relationship between the velocity and the real part of the complex parameter ξ_1. (b) The spectral parameter is written as $\lambda_1 = a_1 + ib_1$. This clearly shows a nonlinear relation between the velocity and spectral parameter. Therefore, we introduce the parameters ξ_j to simplify our soliton solution, which is also much more convenient for discussing the soliton's physical properties. The white line corresponds to $w_1 \neq 0$ or $b_1 \neq 0$.

of Eq. (A6) can be re-expressed as

$$\tau_{j1} = -\frac{1}{2}\left[\xi_j - \frac{1}{\xi_j}\right], \quad \tau_{j2} = -\frac{1}{2}\left[\xi_j + \frac{1}{\xi_j}\right],$$
$$\tau_{j3} = -\frac{1}{2}\left[\xi_j + \frac{1}{\xi_j}\right], \quad \tau_{j4} = \frac{1}{2}\left[\frac{1}{\xi_j} - \xi_j\right].$$

To simplify the solution forms, we can set the coefficients ϕ_{j1}, ϕ_{j2}, and ϕ_{j3} to

$$c_{j1} = 1, \tag{A19}$$

$$c_{j2} = \frac{\xi_j + 1}{\xi_j}\sqrt{1 - |\xi_j|^2}\alpha_j, \tag{A20}$$

$$c_{j3} = \frac{\xi_j + 1}{\xi_j}\sqrt{1 - |\xi_j|^2}\beta_j, \tag{A21}$$

where α_j and β_j are arbitrary constants. Then, the specific solution Eq. (A11) of spectrum problem Eq. (A2) at λ_j can be re-expressed as the following form:

$$\psi_j = \begin{pmatrix} \psi_{j1} \\ \psi_{j2} \\ \psi_{j3} \\ \psi_{j4} \end{pmatrix} = \begin{pmatrix} (1+\xi_j)\phi_{j1} \\ (1+\frac{1}{\xi_j})\phi_{j1}e^{-it} \\ \phi_{j2} \\ \phi_{j3} \end{pmatrix}. \tag{A22}$$

Then, we can obtain the DVDS solution in the first component of $Q[2]$ and the bright solitons in the other two components by performing the following twofold DT processes. For the first-step DT Eq. (A12), the spectral parameters are $\lambda_1 = \frac{1}{2}(\xi_1 + 1/\xi_1)$ and $\xi_1 = -v_1 + iw_1$, and the eigenfunction is constrained by $\psi_{13} = \phi_{12} = 0$, i.e., $\alpha_1 = 0$ (or the eigenfunction $\psi_{14} = \phi_{13} = 0$, i.e., $\beta_1 = 0$). For the second-step DT Eq. (A13), the spectral parameters are $\lambda_2 = \frac{1}{2}(\xi_2 + 1/\xi_2)$ and $\xi_2 = -v_1 + iw_2$, and the eigenfunction is constrained by $\psi_{24} = \phi_{23} = 0$, i.e., $\beta_2 = 0$ (or the eigenfunction $\psi_{23} = \phi_{23} = 0$, i.e., $\alpha_2 = 0$). The simplified solution for $Q[2]$ Eq. (A13) is presented in Eq. (2), where $\beta_1 = 0$, $\alpha_2 = 0$, α_1 and β_2 are nonzero constants. The parameter v_1 is the velocity, and w_1 and w_2 are the width-dependent parameters for DVDSs. It should also be mentioned that when the real parts of ξ_1 and ξ_2 are not equal, the solution Eq. (A13) is related to the incoherent interaction of incoherent solitons, as reported in Ref. [24]. To get the DVDS-related nondegenerate solitons, we choose the same real parts for ξ_1 and ξ_2, based on the formation mechanism of nondegenerate solitons [24].

To study the collision dynamics of DVDSs, further iterations are needed. For example, we can investigate the collision between a DVDS and an SVDS by performing a third-step DT with $\lambda_3 = \frac{1}{2}(\xi_3 + 1/\xi_3)$ and $\xi_3 = -v_2 + iw_3$. We employ ψ_3, which is mapped to $\psi_3[2] = (T[2]\psi_3[1])|_{\lambda=\lambda_3}$ with $\psi_3[1] = (T[1]\psi_3)|_{\lambda=\lambda_3}$:

$$\psi[3] = T[3]\psi[2], T[3] = \mathbb{I} + \frac{\lambda_3^* - \lambda_3}{\lambda - \lambda_3^*}\frac{\psi_3[2]\psi_3[2]^\dagger\Lambda}{\psi_3[2]^\dagger\Lambda\psi_3[2]},$$
$$Q[3] = Q[2] + (\lambda_3 - \lambda_3^*)\left[\sigma_3, \frac{\psi_3[2]\psi_3[2]^\dagger\Lambda}{\psi_3[2]^\dagger\Lambda\psi_3[2]}\right]. \tag{A23}$$

For this case, we constrain the eigenfunctions $\psi_{33} \neq 0$ and $\psi_{34} \neq 0$, i.e., $\alpha_3 \neq 0$, $\beta_3 \neq 0$, and the eigenfunctions ψ_1 and ψ_2 are the same as in the first-step and second-step DT. A typical example of this case is shown in Figs. 5(a1)–5(a3), demonstrating a striking collision process for which a DVDS is transformed into a breather after colliding with an SVDS.

Naturally, by performing a fourth-step DT, one can investigate the interaction between two DVDSs. Before performing this iteration, the eigenfunctions of ψ_3 in the third-step DT Eq. (A23) should be made to satisfy the constraint conditions where the eigenfunction $\psi_{34} = \phi_{33} = 0$, i.e., $\beta_3 = 0$ (or the eigenfunction $\psi_{33} = \phi_{32} = 0$, i.e., $\alpha_3 = 0$). Then, we employ ψ_4, which is mapped to $\psi_4[3] = (T[3]\psi_4[2])|_{\lambda=\lambda_4} = (T[3]T[2]T[1]\psi_4)|_{\lambda=\lambda_4}$. Then, the two DVDS solutions can be obtained as follows with the spectral parameters $\lambda_4 = \frac{1}{2}(\xi_4 + 1/\xi_4)$ and $\xi_4 = -v_2 + iw_4$, and we can constrain the eigenfunction $\psi_{43} = \phi_{42} = 0$, i.e., $\alpha_4 = 0$ (or the eigenfunction $\psi_{44} = \phi_{43} = 0$, i.e., $\beta_4 = 0$):

$$Q[4] = Q[3] + (\lambda_4 - \lambda_4^*)\left[\sigma_3, \frac{\psi_4[3]\psi_4[3]^\dagger\Lambda}{\psi_4[3]^\dagger\Lambda\psi_4[3]}\right]. \tag{A24}$$

In the four-component case, the TVDS can also be obtained by performing the above developed DT with threefold iterations. We do not show the detailed derivation for this process herein. The simplified solution for TVDS is presented in Eq. (10).

In general, the n-fold Darboux matrix can be constructed in the following form:

$$\mathbf{T}_n = \mathbb{I} + \mathbf{Y}_n\mathbf{M}_n^{-1}(\lambda\mathbb{I} - \mathbf{D}_n)^{-1}\mathbf{Y}_n^\dagger\Lambda, \tag{A25}$$

with

$$\mathbf{Y}_n = [|\psi_1\rangle, |\psi_2\rangle, \cdots, |\psi_n\rangle] = \begin{bmatrix} \Psi_1 \\ \Psi_2 \end{bmatrix},$$
$$\mathbf{D}_n = \mathrm{diag}(\lambda_1^*, \lambda_2^*, \cdots, \lambda_n^*),$$
$$\mathbf{M}_n = \left(\frac{\langle\psi_i|\psi_j\rangle}{\lambda_i^* - \lambda_j}\right)_{1\leqslant i,j\leqslant n},$$

Ψ_1 is a $1 \times n$ matrix, and Ψ_2 is an $N \times n$ matrix. The Bäcklund transformation between the old potential functions and the new functions is expressed as follows:

$$\mathbf{q}[n] = \mathbf{q} + 2\Psi_2 \mathbf{M}^{-1} \Psi_1^{\dagger}. \tag{A26}$$

APPENDIX B: THE EXPLICIT EXPRESSIONS FOR $m_i, f_i, g_i, h_i, \delta_i, \rho_i, \vartheta_i, \varrho_i, x_i$, AND d_i IN ASYMPTOTIC ANALYSIS EXPRESSIONS

The explicit expressions of m_i in the DVDS-related vector soliton solutions Eq. (4) are

$$\begin{aligned}
m_1 &= \frac{(w_1 - w_2)^2}{(w_1 + w_2)^2} |y_{13}|^2 |y_{23}|^2, \\
m_2 &= \alpha_1^2 \beta_2^2 |z_{13}|^2 |z_{23}|^2, \\
m_3 &= \alpha_1^2 |y_{23}|^2 |z_{13}|^2, \\
m_4 &= \beta_2^2 |y_{13}|^2 |z_{23}|^2.
\end{aligned}$$

The explicit expressions of f_i in Eq. (4a) are

$$\begin{aligned}
f_1 &= \frac{\xi_1^* \xi_2^* \xi_3^* (w_1 - w_2)^2}{\xi_1 \xi_2 \xi_3 (w_1 + w_2)^2} |y_{13}|^2 |y_{23}|^2, \\
f_2 &= \frac{\xi_3^*}{\xi_3} \alpha_1^2 \beta_2^2 |z_{13}|^2 |z_{23}|^2, \\
f_3 &= \frac{\xi_1^* \xi_3^*}{\xi_1 \xi_3} \beta_2^2 |y_{13}|^2 |z_{23}|^2, \\
f_4 &= \frac{\xi_2^* \xi_3^*}{\xi_2 \xi_3} \alpha_1^2 |y_{23}|^2 |z_{13}|^2.
\end{aligned}$$

The explicit expressions of g_i in Eq. (4b) are

$$\begin{aligned}
g_1 &= \alpha_1 r_1 \xi_1^{-1} y_{13}^* z_{31}, \\
g_2 &= \frac{w_1 - w_2}{w_1 + w_2} |y_{23}|^2, \\
g_3 &= \beta^2 |z_{23}|^2.
\end{aligned}$$

The explicit expressions of h_i in Eq. (4c) are

$$\begin{aligned}
h_1 &= \beta_2 r_2 \xi_2^{-1} y_{32}^* z_{32}, \\
h_2 &= \frac{w_1 - w_2}{w_1 + w_2} |y_{13}|^2, \\
h_3 &= -\alpha_1^2 |z_{13}|^2,
\end{aligned}$$

where

$$\varpi_{ij} = (\xi_i - \xi_j^*)(\xi_i \xi_j^* - 1), \ \eta_{ij} = (\xi_i - \xi_j)(\xi_i \xi_j - 1),$$

$$r_i = (\xi_i - \xi_i^*)\sqrt{1 - |\xi_i|^2}, z_{ij} = \xi_i^* - \xi_j, y_{ij} = \xi_i - \xi_j.$$

The explicit expressions of ϱ_i in the vector breather solutions Eq. (5) are

$$\begin{aligned}
\varrho_1 &= (\lambda_1 - \lambda_1^*)(\lambda_2 - \lambda_2^*), \\
\varrho_2 &= (u_2 n_2^* - u_1 n_1^*)(u_4^* n_3 + u_3^* n_4), \\
\varrho_3 &= (|n_1|^2 - |n_2|^2)(|u_1|^2 - |u_2|^2)|\lambda_1 - \lambda_2^*|^2 \\
&\quad + |n_1^* u_1 - n_2^* u_2|^2 \varrho_1, \\
\varrho_4 &= (|n_3|^2 + |n_4|^2)(|u_3|^2 + |u_4|^2)|\lambda_1 - \lambda_2^*|^2 \\
&\quad + |n_3^* u_4 + n_4^* u_3|^2 \varrho_1, \\
\varrho_5 &= |\lambda_1 - \lambda_2^*|^2 (|n_2|^2 - |n_1|^2)(|u_3|^2 + |u_4|^2), \\
\varrho_6 &= |\lambda_1 - \lambda_2^*|^2 (|u_2|^2 - |u_1|^2)(|n_3|^2 + |n_4|^2).
\end{aligned}$$

The explicit expressions of δ_i in Eq. (5a) are

$$\begin{aligned}
\delta_1 &= (u_4^* n_3 + u_3^* n_4)[n_2^* u_2 - u_1 n_1^* + 2u_2 n_1^* (\lambda_1 - \lambda_2^*)]\varrho_1, \\
\delta_2 &= (u_4 n_3^* + u_3 n_4^*)[n_2 u_2^* - u_1^* n_1 - 2u_1^* n_2 (\lambda_1^* - \lambda_2)]\varrho_1, \\
\delta_3 &= (|n_1|^2 - |n_2|^2)(|u_1|^2 - |u_2|^2)|\lambda_1 - \lambda_2^*|^2 \\
&\quad + |n_1^* u_1 - n_2^* u_2|^2 \varrho_1 \\
&\quad + i4u_1^* u_2 \lambda_1^i [|n_2|^2 (\lambda_1 - \lambda_2)(\lambda_1^* - \lambda_2) \\
&\quad + |n_1|^2 (\lambda_2^* - \lambda_1^*)(\lambda_1 - \lambda_2^*)] \\
&\quad + i4n_1^* n_2 \lambda_2^i [|u_2|^2 (\lambda_1 - \lambda_2)(\lambda_1 - \lambda_2^*) \\
&\quad + |u_1|^2 (\lambda_2^* - \lambda_1^*)(\lambda_1^* - \lambda_2)], \\
\delta_4 &= (|n_3|^2 + |n_4|^2)(|u_4|^2 + |u_3|^2)|\lambda_1 - \lambda_2^*| \\
&\quad + |n_3^* u_4 + n_4^* u_3|^2 \varrho_1, \\
\delta_5 &= (|u_4|^2 + |u_3|^2)|\lambda_1 - \lambda_2^*|^2 [|n_2|^2 \\
&\quad - |n_1|^2 + 2n_1^* n_2 (\lambda_2 - \lambda_2^*)], \\
\delta_6 &= (|n_3|^2 + |n_4|^2)|\lambda_1 - \lambda_2^*|^2 [|u_2|^2 - |u_1|^2 \\
&\quad + 2u_1^* u_2 (\lambda_1 - \lambda_1^*)].
\end{aligned}$$

The explicit expressions of ρ_i in Eq. (5b) are

$$\begin{aligned}
\rho_1 &= u_4 (\lambda_1 - \lambda_2^*)\{u_1^*[|n_1|^2 (\lambda_2^* - \lambda_1^*) + |n_2|^2 (\lambda_1^* - \lambda_2)] \\
&\quad + u_2^* n_1^* n_2 (\lambda_2 - \lambda_2^*)\}, \\
\rho_2 &= u_1^* (\lambda_1^* - \lambda_2)\{u_4[|n_3|^2 (\lambda_1 - \lambda_2) + |n_4|^2 (\lambda_1 - \lambda_2^*)] \\
&\quad + u_3 n_3 n_4^* (\lambda_2^* - \lambda_2)\}, \\
\rho_3 &= n_3 (\lambda_1^* - \lambda_2)\{n_1^*[|u_2|^2 (\lambda_1 - \lambda_2^*) + |u_1|^2 (\lambda_2^* - \lambda_1^*)] \\
&\quad + n_2^* u_1^* u_2 (\lambda_1^* - \lambda_2)\}, \\
\rho_4 &= n_1^* (\lambda_1 - \lambda_2^*)\{n_3[|u_4|^2 (\lambda_1 - \lambda_2) + |u_3|^2 (\lambda_1^* - \lambda_2)] \\
&\quad + n_4 u_3^* u_4 (\lambda_1 - \lambda_1^*)\}.
\end{aligned}$$

The explicit expressions of ϑ_i in Eq. (5c) are

$$\begin{aligned}
\vartheta_1 &= u_3 (\lambda_2^* - \lambda_1)\{u_1^*[|n_1|^2 (\lambda_1^* - \lambda_2^*) + |n_2|^2 (\lambda_2 - \lambda_1^*)] \\
&\quad + u_2^* n_1^* n_2 (\lambda_2^* - \lambda_2)\}, \\
\vartheta_2 &= u_1^* (\lambda_1^* - \lambda_2)\{u_3[|n_3|^2 (\lambda_1 - \lambda_2^*) + |n_4|^2 (\lambda_1 - \lambda_2)] \\
&\quad + n_4 n_3^* u_4 (\lambda_2^* - \lambda_2)\}, \\
\vartheta_3 &= n_4 (\lambda_1^* - \lambda_2)\{n_1^*[|u_1|^2 (\lambda_2^* - \lambda_1^*) + |u_2|^2 (\lambda_1 - \lambda_2^*)] \\
&\quad + n_2^* u_1^* u_2 (\lambda_1^* - \lambda_1)\}, \\
\vartheta_4 &= n_1^* (\lambda_1 - \lambda_2^*)\{n_4[|u_4|^2 (\lambda_1^* - \lambda_2) + |u_3|^2 (\lambda_1 - \lambda_2)] \\
&\quad + n_3 u_3 u_4^* (\lambda_1 - \lambda_1^*)\},
\end{aligned}$$

where

$$\begin{aligned}
u_1 &= 1 + \xi_1, u_2 = 1 + \xi_1^{-1}, \\
n_1 &= 1 + \xi_2, n_2 = 1 + \xi_2^{-1}, \\
u_3 &= -\frac{\alpha_1 \alpha_3 \beta_3 s_1 \varpi_{33}}{(\alpha_3^2 + \beta_3^2)\xi_3 \varpi_{13}},
\end{aligned}$$

$$n_3 = -\frac{\alpha_3\beta_2\beta_3 s_2\varpi_{33}}{(\alpha_3^2+\beta_3^2)\xi_3\varpi_{23}},$$
$$u_4 = \frac{\alpha_1 s_1(\alpha_3^2\xi_3^*\eta_{13}+\beta_3^2\xi_3\varpi_{13})}{(\alpha_3^2+\beta_3^2)\xi_1\xi_3\varpi_{13}},$$
$$n_4 = \frac{\beta_2 s_2(\beta_3^2\xi_3^*\eta_{23}+\alpha_3^2\xi_3\varpi_{23})}{(\alpha_3^2+\beta_3^2)\xi_2\xi_3\varpi_{23}},$$

with

$$s_i = (1+\xi_i)\sqrt{1-|\xi_i|^2}.$$

The explicit expressions of x_i and d_i in the fundamental DBBS solutions Eqs. (7) and (8) are

$$d_1 = \frac{1}{2}\ln x_1, \quad x_1 = \alpha_3^2\frac{|\eta_{13}|^2}{|\varpi_{13}|^2}+\beta_3^2\frac{|\eta_{23}|^2}{|\varpi_{23}|^2},$$
$$d_2 = \frac{1}{2}\ln x_2, \quad x_2 = \frac{(\alpha_3^2+\beta_3^2)|z_{13}|^2|z_{23}|^2}{|y_{13}|^2|y_{23}|^2}.$$

APPENDIX C: THE EXPLICIT EXPRESSIONS FOR η_i AND p_i IN EQ. (10)

The expressions of η_i and p_i in the TVDS solutions Eq. (10) are given by following:

$$\eta_1 = (w_1-w_2)^2(w_1-w_3)^2(w_2-w_3)^2,$$
$$\eta_2 = (w_1+w_2)^2(w_2-w_3)^2(w_1+w_3)^2,$$
$$\eta_3 = (w_1+w_2)^2(w_1-w_3)^2(w_2+w_3)^2,$$
$$\eta_4 = (w_1-w_2)^2(w_1+w_3)^2(w_2+w_3)^2,$$
$$\eta_5 = (w_1+w_2)^2(w_1+w_3)^2(w_2+w_3)^2,$$
$$p_1 = (w_1^2-w_2^2)(w_1^2-w_3^2)(w_2-w_3)^2,$$
$$p_2 = (w_1+w_2)^2(w_1^2-w_3^2)(w_2+w_3)^2,$$
$$p_3 = (w_1^2-w_2^2)(w_1+w_3)^2(w_2+w_3)^2,$$
$$p_4 = (w_2^2-w_1^2)(w_1-w_3)^2(w_2^2-w_3^2),$$
$$p_5 = (w_1+w_2)^2(w_1+w_3)^2(w_2^2-w_3^2),$$
$$p_6 = (w_1-w_2)^2(w_1^2-w_3^2)(w_2^2-w_3^2).$$

[1] P. G. Drazin and R. S. Johnson, *Solitons: An Introduction* (Cambridge University Press, Cambridge, UK, 1989).

[2] P. G. Kevrekidis, D. J. Frantzeskakis, and R. Carretero-González, *Emergent Nonlinear Phenomena in Bose-Einstein Condensates: Theory and Experiment* (Springer, Berlin, 2008).

[3] D. J. Frantzeskakis, Dark solitons in atomic Bose-Einstein condensates: From theory to experiments, J. Phys. A: Math. Theor. **43**, 213001 (2010).

[4] P. Öhberg and L. Santos, Dark Solitons in a Two-Component Bose-Einstein Condensate, Phys. Rev. Lett. **86**, 2918 (2001).

[5] T. Busch and J. R. Anglin, Dark-Bright Solitons in Inhomogeneous Bose-Einstein Condensates, Phys. Rev. Lett. **87**, 010401 (2001).

[6] J. Ieda, T. Miyakawa, M. Wadati, Matter-Wave Solitons in an $F = 1$ Spinor Bose-Einstein Condensate, J. Phys. Soc. Jpn. **73**, 2996 (2004).

[7] F Kh. Abdullaev, A. Gammal, A. M. Kamchatnov and L. Tomio, Dynamics of bright matter wave solitons in Bose-Einstein condensate, Int. J. Mod. Phys. B **19**, 3415 (2005).

[8] C. Becker, S. Stellmer, P. Soltan-Panahi, S. Dörscher, M. Baumert, E.-M. Richter, J. Kronjäger, K. Bongs, and K. Sengstock, Oscillations and interactions of dark and dark-bright solitons in Bose-Einstein condensates, Nat. Phys. **4**, 496 (2008).

[9] X.-F. Zhang, X.-H. Hu, X.-X. Liu and W. M. Liu, Vector solitons in two-component Bose-Einstein condensates with tunable interactions and harmonic potential, Phys. Rev. A **79**, 033630 (2009).

[10] M. A. Hoefer, J. J. Chang, C. Hamner, and P. Engels, Dark-dark solitons and modulational instability in miscible two-component Bose-Einstein condensates, Phys. Rev.A **84**, 041605(R) (2011).

[11] C. Hamner, J. J. Chang, P. Engels, and M. A. Hoefer, Generation of Dark-Bright Soliton Trains in Superfluid-Superfluid Counterflow, Phys. Rev. Lett. **106**, 065302 (2011).

[12] I. Danaila, M. A. Khamehchi, V. Gokhroo, P. Engels, and P. G. Kevrekidis, Vector dark-antidark solitary waves in multicomponent Bose-Einstein condensates, Phys. Rev. A **94**, 053617 (2016).

[13] M. O. D. Alotaibi and L. D. Carr, Dynamics of dark-bright vector solitons in Bose-Einstein condensates, Phys. Rev. A **96**, 013601 (2017).

[14] I. Morera, A. Muñoz Mateo, A. Polls, and B. Juliá-Díaz, Dark-dark-soliton dynamics in two density-coupled Bose-Einstein condensates, Phys. Rev. A **97**, 043621 (2018).

[15] T. M. Bersano, V. Gokhroo, M. A. Khamehchi, J. D'Ambroise, D. J. Frantzeskakis, Three-Component Soliton States in Spinor $F = 1$ Bose-Einstein Condensates, Phys. Rev. Lett. **120**, 063202 (2018).

[16] S. Lannig, C.-M. Schmied, M. Prüfer, P. Kunkel, R. Strohmaier, H. Strobel, T. Gasenzer, P. G. Kevrekidis and M. K. Oberthaler, Collisions of Three-Component Vector Solitons in Bose-Einstein Condensates, Phys. Rev. Lett. **125**, 170401 (2020).

[17] L.-C. Zhao, W. Wang, Q. Tang, Z.-Y. Yang, W.-L. Yang, and J. Liu, Spin soliton with a negative-positive mass transition, Phys. Rev. A **101**, 043621 (2020).

[18] S. K. Adhikari, Stable multi-peak vector solitons in spin-orbit coupled spin-1 polar condensates, Physica E **118**, 113892 (2020).

[19] K. Tai, A. Hasegawa, and A. Tomita, Observation of Modulational Instability in Optical Fibers, Phys. Rev. Lett. **56**, 135 (1986).

[20] Y. S. Kivshar and B. Luther-Davies, Dark optical solitons: Physics and applications, Phys. Rep. **298**, 81 (1998).

[21] Y. S. Kivshar and G. P. Agrawal, *Optical Solitons: From Fibers to Photonic Crystals* (Academic, New York, 2003).

[22] L.-C. Zhao, Y.-H. Qin, C. Lee and J. Liu, Classification of dark solitons via topological vector potentials, Phys. Rev. E **103**, L040204 (2021).

[23] S. Stalin, R. Ramakrishnan, M. Senthilvelan, and M. Lakshmanan, Nondegenerate Solitons In Manakov System, Phys. Rev. Lett. **122**, 043901 (2019).

[24] Y.-H. Qin, L.-C. Zhao, and L. Ling, Nondegenerate bound-state solitons in multicomponent Bose-Einstein condensates, Phys. Rev. E **100**, 022212 (2019).

[25] S. Stalin, R. Ramakrishnan, and M. Lakshmanan, Nondegenerate soliton solutions in certain coupled nonlinear Schrödinger systems, Phys. Lett. A **384**, 126201 (2020).

[26] R. Ramakrishnan, S. Stalin, and M. Lakshmanan, Nondegenerate Solitons and their Collisions in Manakov System, Phys. Rev. E **102**, 042212 (2020).

[27] V. E. Zakharov and A. B. Shabat, Interaction between solitons in a stable medium, Zh. Eksp. Teor. Fiz. **64**, 1627 (1973) [Sov. Phys.-JETP **37**, 823 (1973)].

[28] K. J. Blow and N. J. Doran, Multiple dark soliton solutions of the nonlinear Schrödinger equation, Phys. Lett. **107**, 55 (1985).

[29] V. B. Matveev and M. A. Salle, *Darboux Transformations and Solitons* (Springer-Verlag, Berlin, 1991).

[30] C. H. Gu, H. S. Hu, and Z. X. Zhou, *Darboux Transformations in Integrable Systems: Theory and Their Applications to Geometry* (Springer, Berlin, 2006).

[31] R. Radhakrishnan and M. Lakshmanan, Bright and dark soliton solutions to coupled nonlinear Schrödinger equations, J. Phys. A: Math. Gen. **28**, 2683 (1995).

[32] A. P. Sheppard, Y. S. Kivshar, Polarized dark solitons in isotropic Kerr media, Phys. Rev. E **55**, 4773 (1997).

[33] Y. Ohta, D.-S. Wang, and J. Yang, General N-dark-dark solitons in the coupled nonlinear Schrödinger equations, Stud. Appl. Math. **127**, 345 (2001).

[34] B.-F. Feng, General N-soliton solution to a vector nonlinear Schrödinger equation, J. Phys. A: Math. Theor **47**, 355203 (2014).

[35] Q. H. Park and H. J. Shin, Systematic construction of multicomponent optical solitons, Phys. Rev. E **61**, 3093 (2000).

[36] T. Kanna and M. Lakshmanan, Exact Soliton Solutions, Shape Changing Collisions, and Partially Coherent Solitons in Coupled Nonlinear Schrödinger equations, Phys. Rev. Lett. **86**, 5043 (2001).

[37] E. V. Doktorov and S. B. Leble, *A Dressing Method in Mathematical Physics* (Springer-Verlag, Berlin, 2007).

[38] N. Akhmediev, W. Krolikowski, and A. W. Snyder, Partially Coherent Solitons of Variable Shape, Phys. Rev. Lett. **81**, 4632 (1998); A. Ankiewicz, W. Krolikowski, and N. N. Akhmediev, Partially coherent solitons of variable shape in a slow Kerr-like medium: Exact solutions, Phys. Rev. E **59**, 6079 (1999) N. Akhmediev and A. Ankiewicz, Multi-soliton complexes, Chaos **10**, 600 (2000).

[39] L. C. Zhao, Z. Y. Yang, and W. L. Yang, Solitons in nonlinear systems and eigen-states in quantum wells, Chin. Phys. B **28**, 010501 (2019).

[40] B. L. Guo, L. Ling, Q. P. Liu, Nonlinear Schrödinger equation: Generalized Darboux transformation and rogue wave solutions, Phys. Rev. E **85**, 026607 (2012).

[41] J. S. He, H. R. Zhang, L. H. Wang, K. Porsezian, and A. S. Fokas, Generating mechanism for higher-order rogue waves, Phys. Rev. E **87**, 052914 (2013).

[42] L. Ling, B. Guo L.-C. Zhao, High-order rogue waves in vector nonlinear Schrödinger equations, Phys. Rev. E **89**, 041201(R) (2014).

[43] C. Liu, Z.-Y. Yang, L.-C. Zhao, and W.-L. Yang, Vector breathers and the inelastic interaction in a three-mode nonlinear optical fiber, Phys. Rev. A **89**, 055803 (2014).

[44] L. Ling, L. C. Zhao, B. Guo, Darboux transformation and multi-dark soliton for N-component nonlinear Schrödinger equations, Nonlinearity **28**, 3243 (2015).

[45] L. Wang, Y.-J. Zhu, F.-H. Qi, M. Li and R. Guo, Modulational instability, higher-order localized wave structures, and nonlinear wave interactions for a nonautonomous Lenells-Fokas equation in inhomogeneous fibers, Chaos **25**, 063111 (2015).

[46] L. D. Landau and E. M. Lifshitz, *Quantum Mechanics* (Nauka, Moscow, 1989).

[47] Y.-H. Qin, Y. Wu, L.-C. Zhao, Z. Y. Yang, Interference properties of two-component matter wave solitons, Chin. Phys. B **29**, 020303 (2020).

[48] N. Akhmediev and A. Ankiewicz, Partially Coherent Solitons on a Finite Background, Phys. Rev. Lett. **82**, 2661 (1999).

[49] M. Vijayajayanthi, T. Kanna, and M. Lakshmanan, Bright-dark solitons and their collisions in mixed N-coupled nonlinear Schrödinger equations, Phys. Rev. A **77**, 013820 (2008).

[50] W. Królikowski, N. Akhmediev, B. Luther-Davies, Darker-than-black solitons: Dark solitons with total phase shift greater than π, Phys. Rev. E **48**, 3980 (1993).

[51] W. Królikowski, B. Luther-Davies, Dark optical solitons in saturable nonlinear media, Opt. Lett. **18**, 188 (1993).

[52] Th. Busch and J. R. Anglin, Motion of Dark Solitons in Trapped Bose-Einstein Condensates, Phys. Rev. Lett. **84**, 2298 (2000).

[53] A. Weller, J. P. Ronzheimer, C. Gross, J. Esteve, and M. K. Oberthaler, Experimental Observation of Oscillating and Interacting Matter Wave Dark Solitons, Phys. Rev. Lett. **101**, 130401 (2008).

[54] J. H. V. Nguyen, P. Dyke, D. Luo, B. A. Malomed and R. G. Hulet, Collisions of matter-wave solitons, Nat. Phys. **10**, 918 (2014).

[55] S. V. Manakov, On the theory of two-dimensional stationary self-focusing of electromagnetic waves, Zh. Eksp. Tecr. Fiz. **65**, 505 (1973) [Sov. Phys. JETP **38**, 248 (1974)]

[56] R. Radhakrishnan, M. Lakshmanan and J. Hietarinta, Inelastic collision and switching of coupled bright solitons in optical fibers, Phys. Rev. E **56**, 2213 (1997).

[57] A. A. Sukhorukov and N. N. Akhmediev, Multisoliton complexes on a background, Phys. Rev. E **61**, 5893 (2000).

[58] A. A. Sukhorukov, A. Ankiewicz and N. N. Akhmediev, Multisoliton complexes in a sea of radition modes, Opt. Commun. **195**, 293 (2001).

[59] R. Ramakrishnan, S. Stalin and M. Lakshmanan, Multihumped nondegenerate fundamental bright solitons in N-coupled nonlinear Schrödinger system, J. Phys. A: Math. Theor. **54**, 14LT01 (2021).